Comprehensive multibody dynamics analysis for rotor aeromechanics predictions in descending flight

J.-S. Park and S. N. Jung
snjung@konkuk.ac.kr
Department of Aerospace Information Engineering
Konkuk University
Seoul, South Korea

ABSTRACT

This paper studies the rotor aeromechanics in descending flight using a nonlinear flexible multibody dynamic analysis code, DYMORE. A freewake model is included in DYMORE to improve the rotor wake modelling. The wind-tunnel test data of the Higher-harmonic Aeroacoustics Rotor Test (HART) II rotor, with and without higher harmonic pitch control (HHC), and the flight test data of the full-scale utility helicopter rotor in descent are used for the aeromechanics correlation at an advance ratio of 0·15. The blade-vortex interaction (BVI) airloads are reasonably predicted for both the HART II and utility helicopter rotors, although some BVI peaks are missed on the advancing sides for both the rotors. The flap deflections and elastic torsion deformations at the blade tip are fairly correlated against the measured data of the HART II rotor. The correlation of blade structural moments for both HART II and utility helicopter rotors are not as good as the lift predictions; however, a reasonable prediction is obtained for the utility helicopter rotor.

Paper No. 3687. Manuscript received 30 November 2010, revised version received 23 May 2011, 2nd version received 4 August 2011, accepted 1 September 2011.

https://doi.org/10.1017/S0001924000006813 Published online by Cambridge University Press

NOMENCLATURE

c	Blade chord length, m or ft
C_T	Thrust coefficient
C_n	Section normal force coefficient
M	Mach number
r	Blade radial station, m or ft
R	Blade radius, m or ft
α	Empirical factor (=1·25643)
θ_{3P}	There-per-rev pitch control magnitude, degrees
δ	Apparent viscosity coefficient
ς	Wake age, degrees
υ	Kinematic viscosity, m^2/s or ft^2/s
σ	Rotor solidity
ψ	Rotor azimuth angle, degrees
ψ_{3P}	three-per-rev pitch control phase, degrees

1.0 INTRODUCTION

The trailed tip vortices produced by preceding rotor blades in descending flight may strike the following blades in the vicinity of the rotor plane. This behaviour is known as the blade-vortex interaction (BVI). The BVI phenomenon produces the unsteady pressure fluctuations with the high frequency on a blade, causing significant rotor noise and vibration. The BVI noise is a particularly serious obstacle for rotorcrafts, especially in civil applications.

Over the past 15 years, significant efforts have been made to improve the understanding of the BVI in descending flights through the flight test for a utility helicopter: UH-60A Airloads Program[1] and the wind-tunnel tests: Higher-harmonic Aeroacoustics Rotor Test (HART) I and II[2,3] and the UH-60A rotor system test at NASA Large Rotor Test Apparatus (LRTA)[4,5]. The flight test data of a utility helicopter were acquired from the NASA/Army UH-60A Airloads Program conducted from 1992 to 1994. The extensive flight test data on blade airloads, structural loads, deformations, rotor performance, and acoustics were attained under various flight conditions, including level flights, transient maneuvers, climb, and descending flights. The HART I and II were conducted in 1994 and 2001, respectively, by researchers from German DLR, French ONERA, US NASA Langley, US Army (AFDD), and Netherlands DNW. For both HART I and II, 40% Mach and dynamically scaled models of the BO-105 hingeless rotors were used in the open-jet anechoic test section of the German-Dutch Wind Tunnel (DNW). Massive amounts of test data[6] were obtained on the BVI airloads, acoustics, rotor wakes, blade deformations, and blade structural loads with and without higher harmonic pitch control (HHC) inputs to reduce the noise and vibration. The full-scale UH-60A rotor system was tested at the National Full-Scale Aerodynamics Complex (NFAC) 80ft by 120ft and the 40ft by 80ft wind tunnels located at NASA Ames Research Center[4,5]. The tests were conducted to improve the rotor performance and reductions of loads, noise, and vibration from the use of an individual blade control (IBC) in hover, low- and high-speed forward flights, and

https://doi.org/10.1017/S0001924000006813 Published online by Cambridge University Press

descending flight conditions. Extensive measurements were made for the rotor performance, blade airloads, structural loads, the BVI noise with and without IBC, and the wind-tunnel test results were compared with the flight test data obtained from the UH-60A Airloads Program.

Along with the rotor tests in descent, significant volume of research have been devoted to investigate the aeromechanics using the rotor comprehensive structural dynamics (CSD)[7], computational fluid dynamics (CFD)[8], and CSD/CFD coupled analysis[9,10]. Nevertheless, the previous prediction efforts show a number of limitations. First, for the HART II rotor, there is a difficulty in conducting a correlation study for the BVI airloads on the entire rotor disk because the airloads were measured only at a single blade station (87% span). In addition, the prediction of blade structural loads, such as the flap bending, lead-lag bending, and torsion moments, were not correlated with the measured data except Ref. 10. Second, for the UH-60A rotor in descent, although the blade structural moments as well as the airloads in the full range of the blade span were correlated between the analysis and measured data, only one rotor comprehensive analysis code, CAMRAD II[11], was used for the CSD analysis alone[7] and for the CSD/CFD coupled analysis[9,10]. Thus, the prediction results were not compared with the results of other rotor CSD codes.

Recently, the nonlinear flexible multibody dynamics analysis codes such as DYMORE[12] and MBDYN[13] have been widely applied to rotorcraft analyses[14-17]. DYMORE is capable of multibody modelling based on an arbitrary topology; thus, it can represent effectively the complex rotor control systems. DYMORE has various multibody elements; rigid bodies, rigid and elastic joints and nonlinear elastic bodies such as beams, plates, and shells based on the finite element method. The geometrically exact beam theory[18] is used for the nonlinear elastic beam. Furthermore, DYMORE has simple aerodynamic models based on the lifting line theory for rotors and wings, and it also allows the coupling analysis with an external CFD code. Although the coupling analysis with the CFD can improve considerably the prediction capability, the stand-alone DYMORE analysis is still important since it is more efficient and fast to obtain the reasonable prediction as compared to the coupling analysis. However, DYMORE's inflow model for the rotor, the finite-state dynamic inflow model[19], is not sufficient to predict precisely the rotor airloads under the edgewise flight conditions. Thus, the freewake model[20] was implemented into DYMORE in order to improve the wake modelling capability[15,16]. The present study differs from the authors' previous work[16] in that[1]: Ref. 16 focused only on the HART II validation while the present work covers also the full-scale utility helicopter rotor in descent[2]; a significant phase-shift problem in the section normal force prediction was observed in Ref. 16 and this has been remedied by improving the blade modelling.

The objective of this paper is to investigate the aeromechanical behaviour of not only the HART II rotor but also a utility helicopter (UH-60A) in descending forward flights using DYMORE[12]. The freewake model is included in DYMORE for more accurate prediction of the BVI airloads. The section normal forces or lifts, blade deformations, and blade structural loads of the rotors are predicted and compared with the measured data. In addition, the present prediction for a utility helicopter rotor in descent is also compared with the previously obtained CAMRAD II analysis results[7,9]. The correlation results demonstrate the prediction capability of DYMORE with the freewake model for the rotor aeromechanics in descending flights.

https://doi.org/10.1017/S0001924000006813 Published online by Cambridge University Press

Table 1
Test conditions in descending forward flight

Cases		μ	α_s	C_T/σ	M_{tip}
HART-II	BL	0·15	4·5°	0·055	0·64
	MN	0·15	4·5°	0·056	0·64
	MV	0·15	4·5°	0·056	0·64
Utility Helicopter		0·15	5·8°	0·065	0·65

Table 2
Higher harmonic pitch control inputs for HART II MN and MV cases

Cases		θ_{3P}	ψ_{3P}
HART II	MN	0·81°	300°
	MV	0·79°	380°

2.0 ANALYTICAL MODELLING

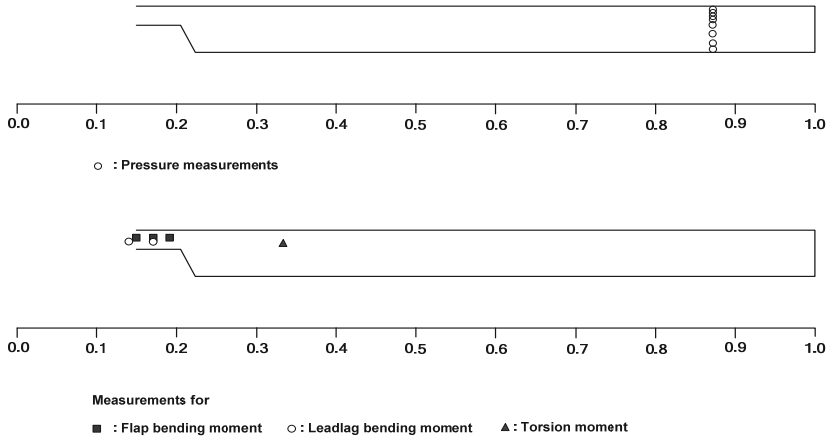
2.1 Test data

For the correlation study of the rotor aeromechanics in descending flight, the four rotor test conditions with an advance ratio μ = 0·15 are considered as summarised in Table 1: the three test cases of the HART II[6], that is, baseline (BL), minimum noise (MN), minimum vibration (MV), and one test case (counter 9812) for a utility helicopter[7,9,10].

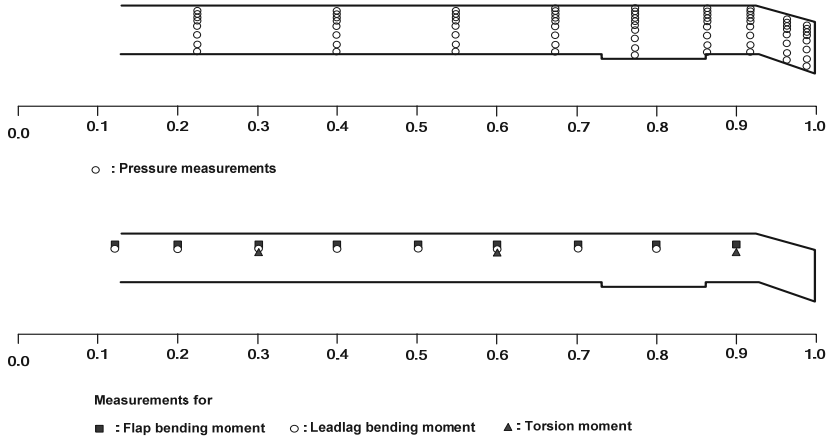
The wind-tunnel test data for the HART II are obtained from Ref. 6. The rotor shaft tilting angle is 5·3°. during the test, but the effective shaft angle, α_s, is 4·5°. after considering the wind-tunnel wall and fuselage effects. The three-per-rev (3P) pitch control inputs given in Table 2 are added to the BL case for the MN and MV cases. Figure 1(a) shows the HART II blade planform with equipments for measuring the airloads and structural loads. The pressure on the reference blade surface was measured at the 87% radial location. The blade position and deformations were measured optically by means of a stereo pattern recognition (SPR) technique. The blade structural loads were measured with the six strain gauges: three for the flap bending moments at r/R = 0·15, 0·17 and 0·19, two for the lead-lag bending moments at r/R = 0·14 and 0·17, and one for the torsion moment at r/R = 0·33. The test data for the section airloads and blade deformations can be obtained from Ref. 6; however the measured blade structural loads are not included in Ref. 6. Thus, the measured blade structural moments for the present correlation are obtained from the previous research[10].

The descending flight condition for a utility helicopter[7,9,10] as given in Table 1 is similar to the HART II test condition. Figure 1(b) shows the blade planform of a utility helicopter rotor along with the equipments to measure the section airloads and the blade structural loads for the flight test: The pressure gauges for the section airloads were installed at the nine blade stations (r/R = 0·225, 0·40, 0·55, 0·675, 0·775, 0·865, 0·92, 0·965, and 0·99). For the blade structural loads, the flap bending moments were measured at r/R = 0·113, 0·2, 0·3, 0·4, 0·5, 0·6, 0·7, 0·8, and 0·9. The lead-lag bending moments were measured at r/R = 0·113, 0·2, 0·3, 0·4, 0·5, 0·6,

https://doi.org/10.1017/S0001924000006813 Published online by Cambridge University Press



(a) HART II



(b) Utility helicopter

Figure 1. Blade planforms with measurement equipments for HART II and utility helicopter rotors.

0·7, and 0·8. The torsion moments were measured at $r/R = 0{\cdot}3$, 0·5, 0·7, and 0·9. It is noted that several strain gauges were broken. In addition, there were no test data available for the blade deformations of a utility helicopter in the given flight condition. The flight test data for the section lifts and the blade structural moments are obtained from Refs 7, 9, and 10 for the correlations in this paper.

2.2 DYMORE modelling

DYMORE modellings of HART II and utility helicopter rotors in descent for the comprehensive multibody dynamics analysis are described in this section.

For the HART II rotor, a total of four nonlinear elastic blades along with a rigid hub are considered. Table 3 shows the general properties of the HART II rotor. The detailed properties

https://doi.org/10.1017/S0001924000006813 Published online by Cambridge University Press

Table 3
General properties of HART II and utility helicopter rotors

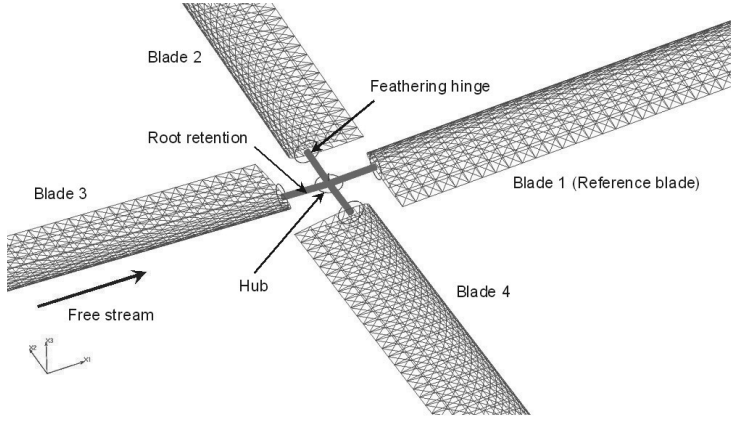
	HART II	Utility Helicopter
Rotor type	Hingeless	Articulated
Scale type	Mach-scale	Full-scale
Planform	Rectangular	Rectangular with tip sweep
Number of blades, N	4	4
Radius, R	2·0m (6·56ft)	8·18m (26·83ft)
Locations of hinges	0·0375R (feathering)	0·0466R (feathering)
		0·0466R (flap)
		0·0466R (leadlag)
Chord length, c	0·121m (0·397ft)	0·534m (1·753ft)*
Solidity, σ	0·0770	0·0832
Built-in twist	–8·0° (linear)	–16·0° (nonlinear)
Sweepback angle	N/A	20° at 0·9286R
Precone angle	2·5°	0·0°
Nominal rotor speed, Ω_{ref}	109·0rad/s	27·02rad/s

* The mean chord length

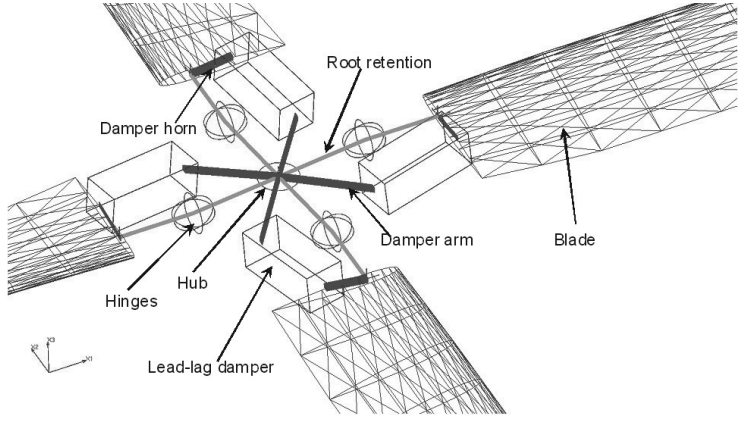
can also be found in Ref. 21. Figure 2(a) illustrates the DYMORE modelling of the HART II rotor system. The present multibody dynamics modelling for the HART II is based on the authors' previous work[16], but some adjustments about the modelling of the blade properties such as elastic axis offsets are made in this paper. For the finite element modelling of the blade, each blade is discretised into ten cubic beam elements. Since the HART II rotor is a hingeless rotor, there is only a feathering hinge that is modeled as a revolute joint. The equivalent torsional spring at the feathering hinge is used to represent the stiffness of the rotor control system. The value of the torsional spring constant is determined appropriately to match the first torsional frequency (T1) at the nominal rotor speed. The hub is modeled as a rigid body and connected to a revolute joint with a prescribed rotational speed. For the aerodynamic loads on the blade, 31 airstations are used with equal spacing on each blade. A C81 table for a NACA20312 airfoil with a tab is also utilised. The HART II rotor is trimmed to match the target values of the rotor thrust, the hub pitching, and rolling moments, all of which are provided by Ref. 6.

Although the measured data for a utility helicopter rotor were obtained from the flight test[1], the present modelling for a utility helicopter considers only isolated rotor system for simplicity. The properties of its main rotor are summarised in Table 3, and the DYMORE modelling for the main rotor system of a utility helicopter is illustrated in Figure 2(b). The configuration data for the main rotor system can be found in Ref. 22. The present multibody modelling includes the root retention, blade, hydraulic lead-lag damper, damper arm, damper horn, and hub. The root retention has three separate segments from the hub to the blade, with three, two, and two cubic beam elements, respectively. Three co-located revolute joints are used between the first two segments to represent the flap, lead-lag, and feathering hinges of the articulated rotor system.

https://doi.org/10.1017/S0001924000006813 Published online by Cambridge University Press



(a) HART II



(b) Utility helicopter

Figure 2. DYMORE modellings for HART II and utility helicopter rotor systems.

The physical characteristics of the hinges are represented by springs and dampers in the joints. The spring constants having the values of 90ft-lbs/deg. are used for both the flap and lead-lag hinges. Like in the HART II rotor modelling, an equivalent torsional spring is attached to the feathering hinge to model the rotor control system stiffness. In the present work, the equivalent torsional spring constant has 1,090ft-lbs/deg. This value represents a stiff pitch link modelling. The modelling with a stiff pitch link is believed to be more realistic than that using a soft pitch link with the value of 363ft-lbs/deg., since the stiff torsional spring constant value (1,090ft-lbs/deg.) was derived from the experiment[26]. In addition, the adjusted damping value of about 44ft-lbs/deg/sec is used at the lag hinge. The blade is discretised into ten cubic beam elements. The sectional properties of the root retention and blade are given in Ref. 23. The damper arm and damper horn are modeled as rigid bodies. The lead-lag damper is modeled as a hydraulic damper[24]; its physical properties are described in Ref. 25. In addition, the equally spaced 68 airstations along with C81-type airfoil tables are used to model the aerodynamic loads on the

https://doi.org/10.1017/S0001924000006813 Published online by Cambridge University Press

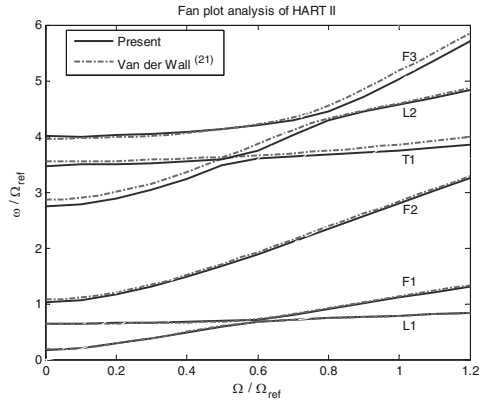


Figure 3. Fan plot analysis result of HART II rotor (Ω_{ref} = 109·00rad/s).

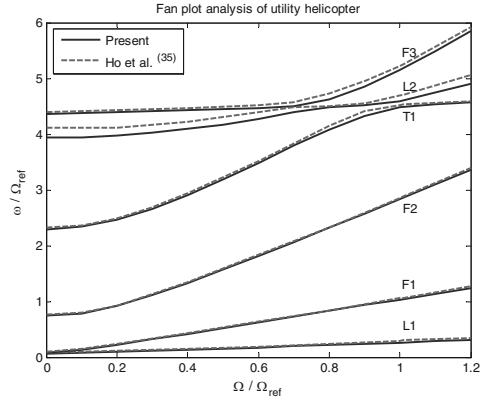


Figure 4. Fan plot analysis result of a utility helicopter (Ω_{ref} = 27·02rad/s).

blade. The airfoil tables are regenerated from the collection of data available in the public domain[22,27-32]. In the trim analysis of the present utility helicopter rotor model, the target hub pitching and rolling moments are not used. Instead, the pitch control angles are adjusted to match the target thrust and the one-per-rev longitudinal and lateral flapping angles are set to zero.

DYMORE calculates the aerodynamic loads at the airstations by using 2D unsteady airfoil theory with the airfoil table lookup. The finite-state dynamic inflow model[19] is originally included as an inflow model for the rotor; however, as mentioned previously, this model is inappropriate for sophisticated rotor aerodynamics predictions. The general freewake model[20] is therefore implemented directly as an integral part of DYMORE to enhance the rotor modelling capability[15,16]. The present freewake model considers a single-tip vortex filament on each lifting line of a rotor, released from each blade tip. A vorticity transport equation is used for the freewake analysis. This equation is then discretised into a set of finite difference equations, which are integrated by a time marching algorithm that is modified for implementation in DYMORE[15]. The trailed near wake is also considered to improve the accuracy of modelling. The detailed explanation of the freewake model is given in Refs 15, 16 and 20. In the present freewake modelling for both the rotors, the growth of the core radius is determined by the relation[33] $r_c(\varsigma) = \sqrt{r_{\text{initial}}^2 + 4\alpha\delta\nu\varsigma/\Omega_{\text{ref}}}$ In this expression, the initial core radii, r_{initial}, at the root and tip of a blade use the values of 1·0c and 0·2c, respectively. The apparent viscosity coefficients[34] δ used for the HART II and a utility helicopter rotor are 1,000 and 10,000, respectively.

3.0 NUMERICAL RESULTS

3.1 Rotor natural frequencies

The rotating frequencies of the lowest six modes of the HART II and utility helicopter rotors in vacuum are predicted and compared with the previous results in order to validate the present structural dynamics modelling of the rotor systems. The collective pitch angle of 0° is used and the rotating speed is increased up to 1·2 times the nominal rotor speed for both the rotors. Figure 3 shows the fan plot analysis of the HART II rotor. The present prediction result by DYMORE shows an acceptable correlation with that in Ref. 21. In particular, the accurate prediction for

https://doi.org/10.1017/S0001924000006813 Published online by Cambridge University Press

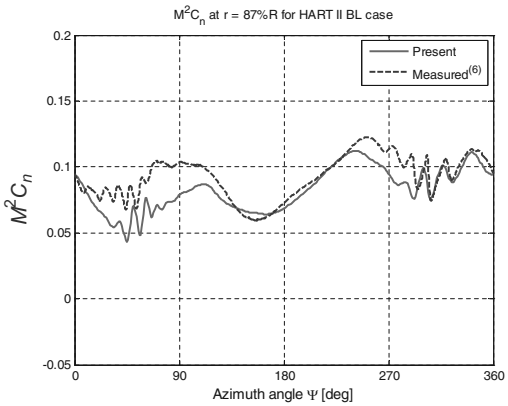


Figure 5. Correlation of section normal forces at 87% span location for HART II BL case.

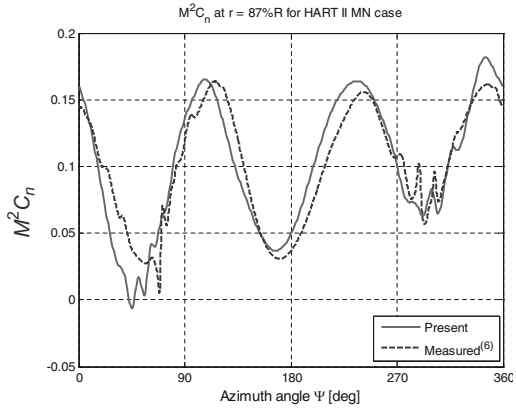


Figure 6. Correlation of section normal forces at 87% span location for HART II MN case.

the first torsional frequency (T1) is quite important in the structural dynamics modelling because the torsional behaviour of the rotor blade is closely related to the lift variation. Figure 4 shows the result of the fan plot analysis of a utility helicopter rotor with the stiff pitch link model. The present frequencies are in excellent agreement with the CAMRAD II predictions in Ref. 35. Thus, the results of the fan plot analysis confirm the sound construction of the current structural dynamics modellings of the HART II and utility helicopter rotors.

3.2 BVI airloads

In this section, the section normal forces or lifts of the four rotor test cases, the HART II BL, MN, MV and a utility helicopter in descent, are predicted and compared with the measured data. The prediction for a utility helicopter is also compared with the previous CAMRAD II results[7,9]. The results of the comparison show the capability of the present prediction on BVI airloads. The similarity and difference in BVI airloads of the four rotor tests in descending flight are also investigated.

3.2.1 HART II

In Fig. 5 the predicted section normal force, M^2C_n, at the 87% blade span of the HART II BL case is compared with the measured data[6]. The present DYMORE analysis with the freewake model predicts well the three-per-rev sectional lift variation. It was one important issue in the HART I program to predict three-per-rev lift variation related to vortex wake modelling. The measured data shows significant lift fluctuations in the first and fourth quadrants. This behaviour occurs since the trailed tip vortices strike the blade again in the rotor plane, resulting in severe BVI phenomena. Although the present analysis misses the first two interactions in the first quadrant, it can make good predictions of lift oscillations with high frequency due to the BVIs. On the retreating side, the present prediction captures the number and magnitude of BVI loadings nicely.

Figure 6 shows the predicted and measured section normal forces, M^2C_n, at the 87% blade span of the HART II MN case. Compared with the BL case, the three-per-rev section lift variations in both the test data and the present prediction become stronger since the three-per-rev HHC inputs given in Table 2 are introduced for this MN case. It is noticeable that the number of

https://doi.org/10.1017/S0001924000006813 Published online by Cambridge University Press

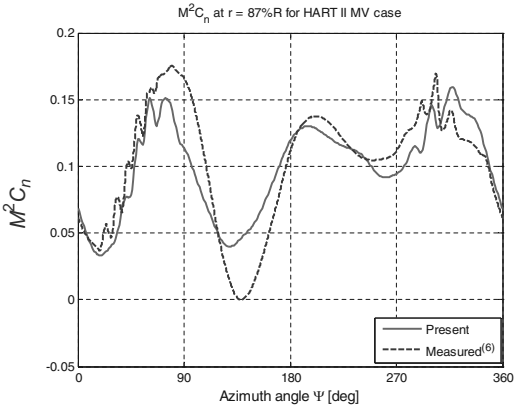
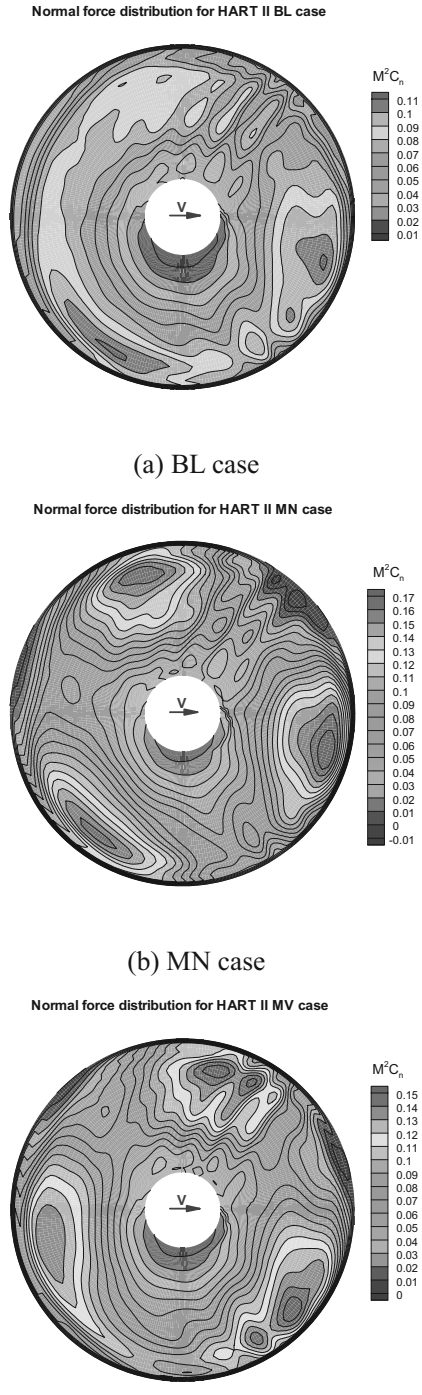


Figure 7. Correlation of section normal forces at 87% span location for HART II MV case.

measured BVI events is reduced significantly. Furthermore, as compared with the BL case, the section lifts of the MN case are increased in the second quadrant in both the measurement and the prediction. In this region, the circulation of the trailed tip vortices could be larger so that the induced velocity becomes increased. This increased induced velocity along with the elastic flap motion will increase the miss-distance which is defined as the vertical distance between the rotor blade and the tip vortices. The miss-distance is one of the driving factors affecting the BVI. In the end, the vortices may pass far away from the blade without causing any significant BVI events. The effect of blade flap motions on the miss-distance will be discussed in a later section. The correlation for the MN case is relatively good for both the advancing side and retreating side, though the predicted lift down in the first quadrant occurs earlier than indicated in the test results.

Figure 7 shows the predicted and measured section normal force, M^2C_n, at the 87% blade span of the HART II MV case. As in the previous MN case, the measured and predicted lifts for the MV case show a more distinct three-per-rev lift variation as compared with the BL case since the MV case also uses the three-per-rev HHC inputs given in Table 2. In contrast with the previous MN case, the measured section lift in the second quadrant becomes decreased to nearly zero. The



(a) BL case

(b) MN case

Figure 8. Predicted normal force distributions over the rotor disk for HART II BL, MN, and MV cases.

https://doi.org/10.1017/S0001924000006813 Published online by Cambridge University Press

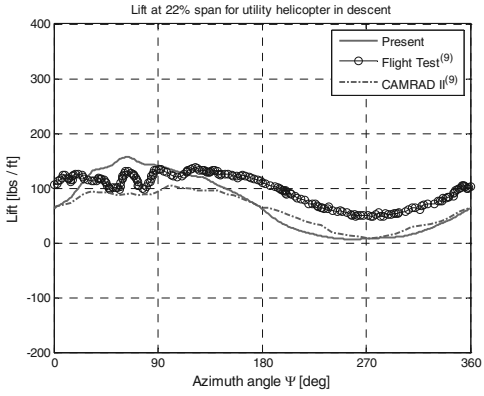
DYMORE prediction captures reasonably the lift fluctuations caused by the BVIs in both the first and fourth quadrants, but over-predicts the magnitude of the section lift in the second quadrant. A moderate phase lag, amounting about 15°, is also observed in the fourth quadrant.

Figure 8 shows the predicted lift contour plots of the HART II BL, MN and MV cases. For the BL case, there are three peaks in the rear portion, advancing side, and retreating side of the rotor disk. In addition, a number of BVI peaks are observed in the first and fourth quadrant of the rotor disk. The BVIs in the advancing side extend more inboard along the blade span, as compared with those in the retreating side. When the lift distribution for the MN case is compared with the BL case, the number of BVI peaks becomes reduced significantly, with the introduction of the three-per-rev HHC inputs. Moreover, there are no pronounced BVI peaks near the blade tip, on the advancing side of the rotor disk. The absence of these peaks is the main reason for the reduced noise emission in the MN case. In contrast to the MN case, the MV cases have a few BVI peaks in the blade tip region on the advancing and retreating sides; however, the peak-to-peak value of M^2C_n is quite similar to that of the MN case.

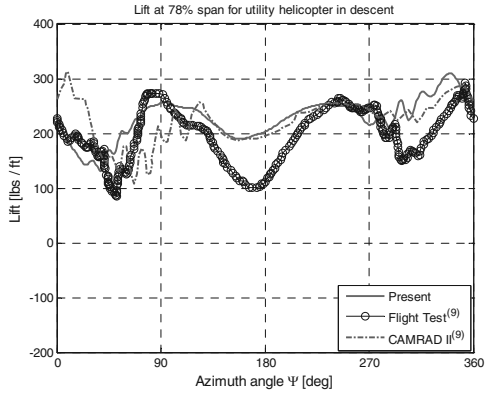
3.2.2 Utility helicopter

Figure 9 shows the comparison of the predicted section lifts of a utility helicopter rotor in descent with the flight test data[9] and the CAMRAD II results with the multiple trailer wake model[9]. Unlike the previous HART II correlation study, the section lifts at the six different blade stations from the blade root to the tip are considered. The measured lift near the blade root shows a one-per-rev variation; however, the lift variations at the outboard from the 68% blade span turn into a three-per-rev variation which shows a 'down-up' impulse on the advancing side and an 'up-down' impulse on the retreating side. In addition, the measured lifts at near the blade tip (87% and 97% blade span locations) show the negative lifts in the front of the rotor disk. In the flight test data, the BVI events on the advancing side are clearly evident at the inboard and mid-span locations of the rotor blade, and the magnitude of the BVI airloads dies out near the blade tip. On the other hand, the BVIs on the retreating side show up from the 55% blade span to the blade tip. The present analysis predicts well the one-per-rev variation of the section lift at the 22% blade span but fails to capture the BVI events in the first quadrant, and neither does the previous CAMRAD II analysis. The section lift at the 55% blade span is predicted reasonably as compared with the measured data; however, some BVI events are not captured in the first quadrant as was the case with the prediction for HART II, and the magnitude of lift fluctuations is under-predicted on both the advancing and retreating sides. The lift prediction at the 68% blade span where the three-per-rev lift variation begins to appear is not as good as the results at the 22% and 55% blade stations since the lift in the second and third quadrants is under-predicted. In addition, the present DYMORE analysis in the first quadrant under-predicts the magnitude of the BVI airloads and misses the first two BVIs, whereas the CAMRAD II result in Ref. 9 show spurious BVI events on the advancing side. However, the section lift variations by the two predictions are quite similar to each other. The BVI airloads on the retreating sides at both the 78% and 87% blade stations are predicted well, but the lifts at around the azimuth angle of 180° are over-predicted. Furthermore, for the section lift on the advancing side at the 78% blade span, like the previous case at the 68% blade span, the present DYMORE analysis misses some BVI peaks while the previous CAMRAD II analysis shows spurious BVI events. The lift at the 97% blade span shows a relatively good correlation, though it fails to show a definite negative lift at around the azimuth angle of 180°. The CAMRAD II result in Ref. 9 demonstrates clearly a negative lift at around the azimuth angle of 180°, but it under-predicts significantly the lift in the first quadrant.

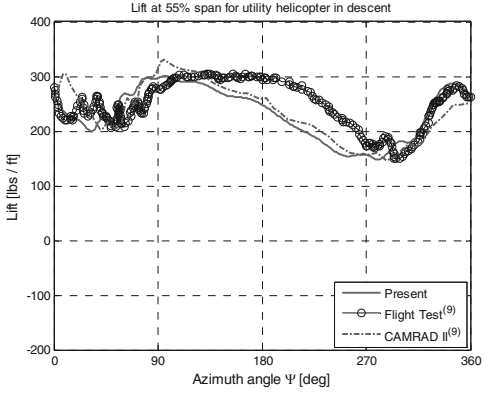
https://doi.org/10.1017/S0001924000006813 Published online by Cambridge University Press



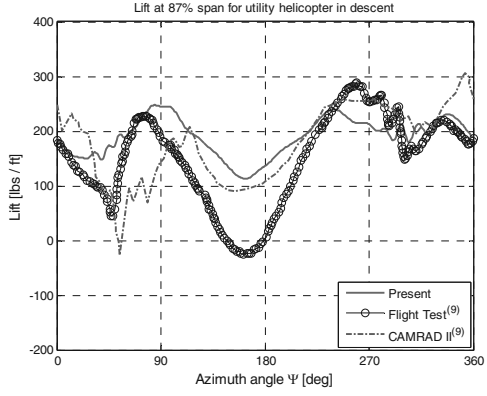
(a) 22% blade span



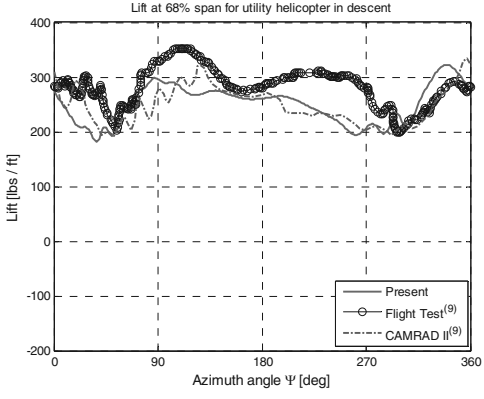
(d) 78% blade span



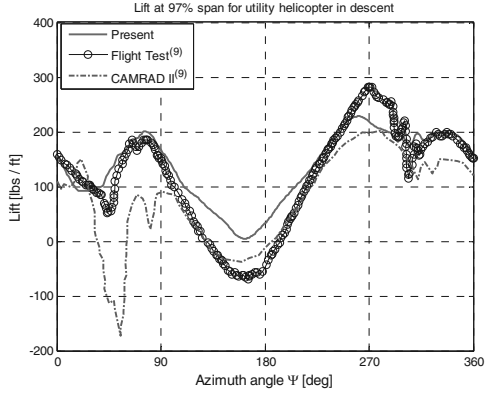
(b) 55% blade span



(e) 87% blade span



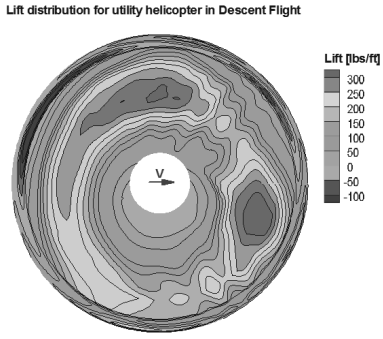
(c) 68% blade span



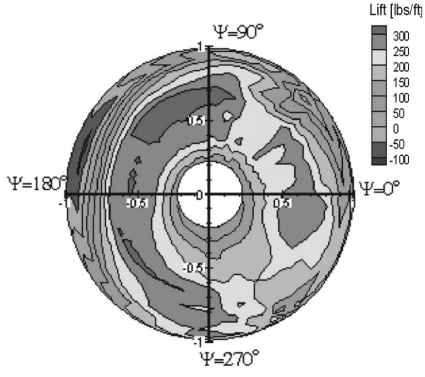
(f) 97% blade span

Figure 9. Correlation of section lifts for a utility helicopter in descent.

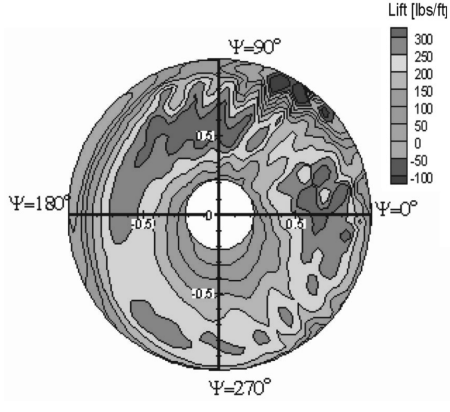
https://doi.org/10.1017/S0001924000006813 Published online by Cambridge University Press



(a) Present prediction

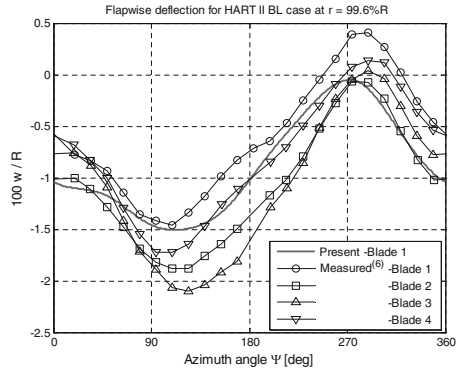


(b) Flight test[7]

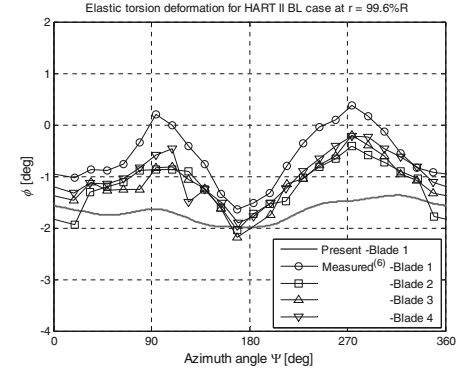


(c) CAMRAD II with multiple trailer wakes[7]

Figure 10. Correlation of lift distribution over the rotor disk for a utility helicopter in descent.



(a) Flap deflection



(b) Elastic torsion deformation

Figure 11. Correlation of blade tip deformations for HART II BL case.

https://doi.org/10.1017/S0001924000006813 Published online by Cambridge University Press

Figure 10 shows the lift distributions of the present prediction by DYMORE, flight test[7] and CAMRAD II result[7]. The DYMORE analysis predicts well the three lift peaks in the after of the rotor disk, and on the advancing and retreating sides. This is quite similar to the characteristic of the normal force peaks for the HART II BL case given in Fig. 8(a). Furthermore, a fairly good prediction is made of the negative lift at the blade tip region in the front of the rotor disk. The comparison of the present DYMORE result with the previous CAMRAD II prediction is also acceptable.

3.3 Blade deformations

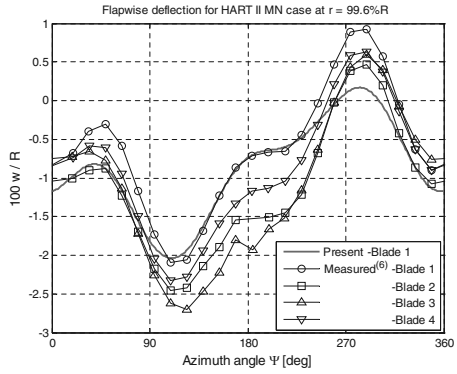
Since there was no available test data of blade deformations for a utility helicopter in the given descending flight condition, the blade deformations for the HART II rotor only are discussed in this section. All the previous HART II prediction analyses showed that the correlations of lead-lag deflection have a significant offset with the measured data; thus, the flap deflection (w) and elastic torsion deformation (φ) at the blade tip for the BL, MN, and MV cases are studied in this paper. The flap deflection was measured without a precone angle, and its positive direction is defined as a flap-up. The elastic torsion deformation is defined without pitch controls and a pretwist, and the positive direction is defined as a nose-up.

Figure 11 gives the flap deflection and elastic torsion deformation at the blade tip for the BL case. The measured flap deflection shows a slight blade-to-blade variation due to dissimilarities. The present prediction for the flap deflection shows a good correlation with the measured data. The measured elastic torsion deformation exhibits substantial blade-to-blade variations, with a mean value difference of 0·6°. The correlation of the predicted elastic torsion deformation is seen to be fair. The maximum deviation is about 1·2°. The peak-to-peak value is significantly under-predicted, as compared with the measured value. A CSD/CFD coupled analysis is desired to enhance the correlation.

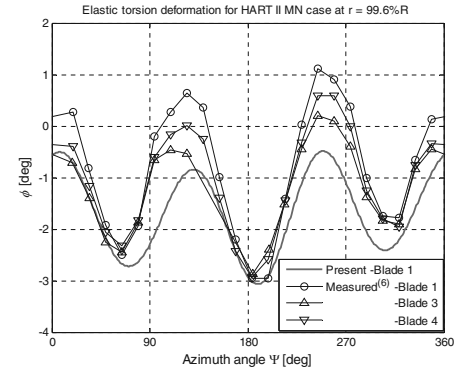
The blade deformations at the tip in the MN case are shown in Fig. 12. The predicted flap deflection is a good match with the measured data, though, as already observed in the BL case, the peak-to-peak magnitude is under-predicted. As discussed previously, the flap deflection at the blade tip is closely related to the miss-distance at the two particular azimuth angles related to the vortex generation and the BVI. The measured data and prediction both show that the blade flaps down at around the azimuth angle of 130° where a tip vortex is generated, whereas the blade flaps up at around the azimuth angle of 60° where the blade and the tip vortex interact. This flap motion increases the miss-distance and, as a result, may reduce the rotor noise emission for the MN case. In the MN case, both the measured and predicted elastic torsion deformations clearly show three-per-rev responses which are due to the introduction of three-per-rev harmonic inputs. This prediction is better than that of the BL case, though the peak-to-peak and mean values are under-predicted in comparison with the measured data.

The correlations of blade deformations at the tip for the MV case are given in Fig. 13. The flap deflection behaviour at the two specified locations of vortex generation and BVI encounter appear almost opposite to that of the MN case since the blade flaps down at around the azimuth angle of 60° whereas the blade flaps up at around the azimuth angle of 130°. The reversed situation reduces the miss-distance for the MV case, causing significant lift fluctuations on the advancing side. The flap deflection is predicted reasonably well but is moderately under-predicted near the azimuth angle of 0°. The predicted elastic torsion deformation shows the three-per-rev variation well, but its peak-to-peak value is significantly under-predicted.

https://doi.org/10.1017/S0001924000006813 Published online by Cambridge University Press

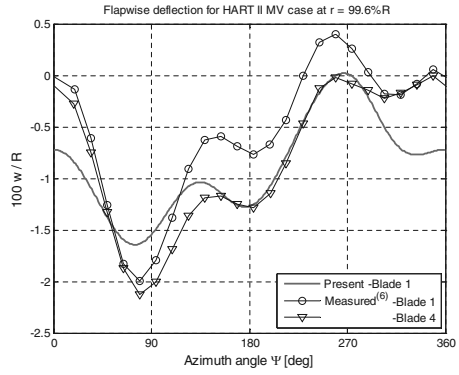


(a) Flap deflection

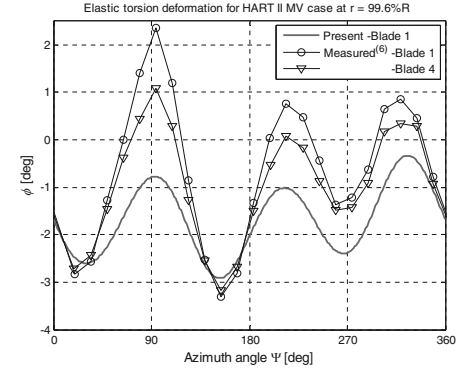


(b) Elastic torsion deformation

Figure 12. Correlation of blade tip deformations for HART II MN case.



(a) Flap deflection



(b) Elastic torsion deformation

Figure 13. Correlation of blade tip deformations for HART II MV case.

3.4 Blade structural loads

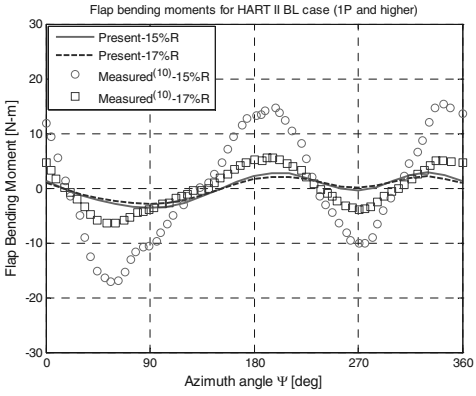
Next, the blade structural loads, such as the flap bending, lead-lag bending and torsion moments, of both the HART-II and utility helicopter rotors are correlated with the measured data. The mean values are removed to compare only with the oscillatory structural loads components. The structural load correlations are not investigated for the entire blade span because both the rotors have some defective strain gauges and the HART II rotor has only a limited installation of strain gauges.

3.4.1 HART II

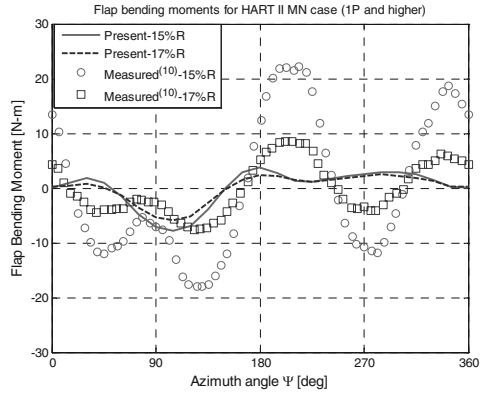
For the HART II rotor, the flap bending moments at $r/R = 0{\cdot}15$ and $0{\cdot}17$, the lead-lag bending moments at $r/R = 0{\cdot}14$ and $0{\cdot}17$, and the torsion moment at $r/R = 0{\cdot}33$ are considered for the correlation of the blade structural loads.

Figure 14 shows the correlation of the blade structural loads in the BL case. The two measured flap bending moments are significantly different, even though they were measured at the two adjacent radial locations. However, the two predicted flap bending moments are

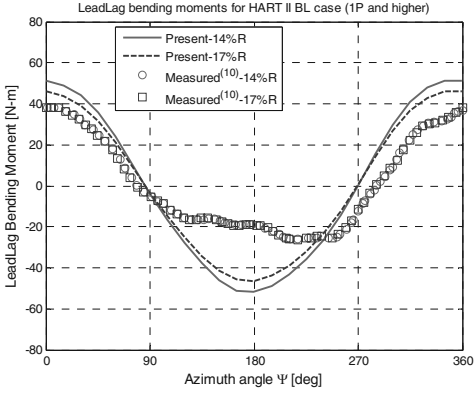
https://doi.org/10.1017/S0001924000006813 Published online by Cambridge University Press



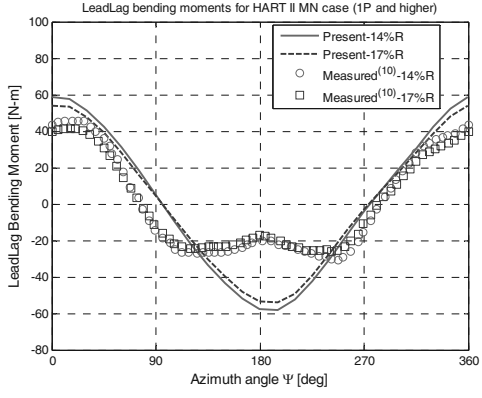
(a) Flap bending moments



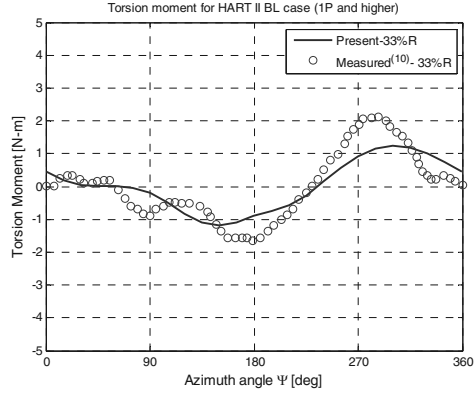
(a) Flap bending moment



(b) Leadlag bending moments

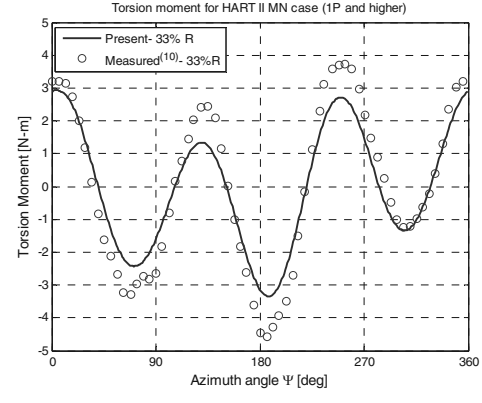


(b) Leadlag bending moments



(c) Torsion moment

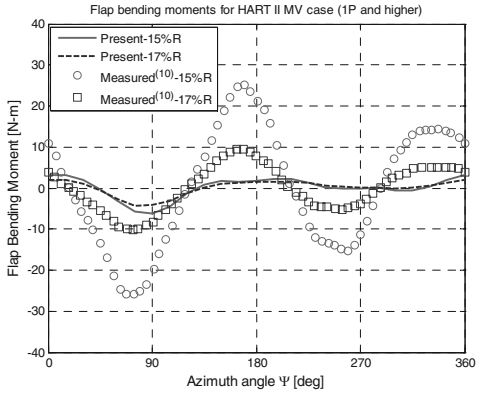
Figure 14. Correlation of blade structural loads for HART II BL case.



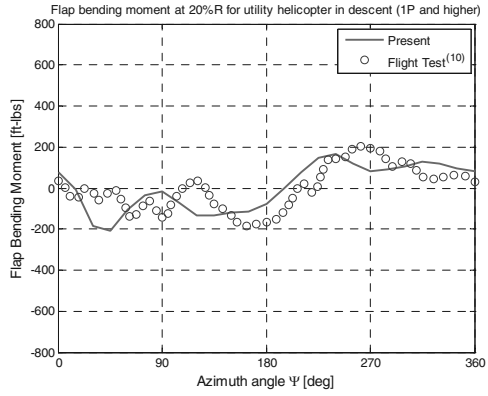
(c) Torsion moment

Figure 15. Correlation of blade structural loads for HART II MN case.

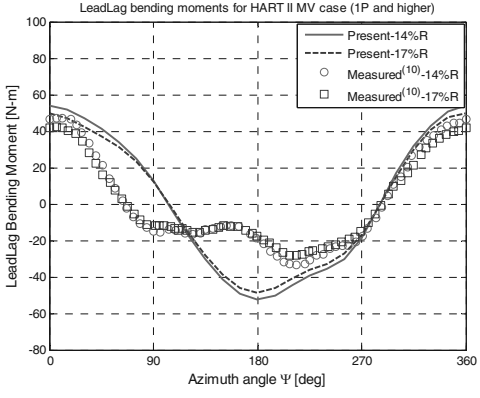
https://doi.org/10.1017/S0001924000006813 Published online by Cambridge University Press



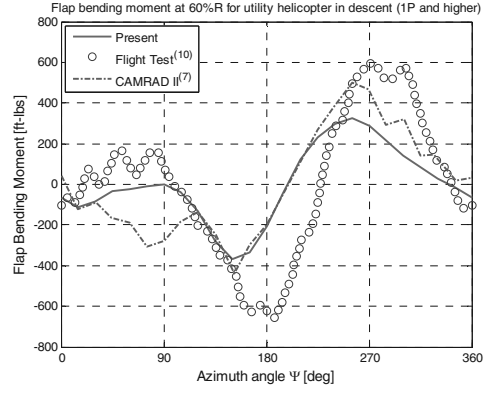
(a) Flap bending moment



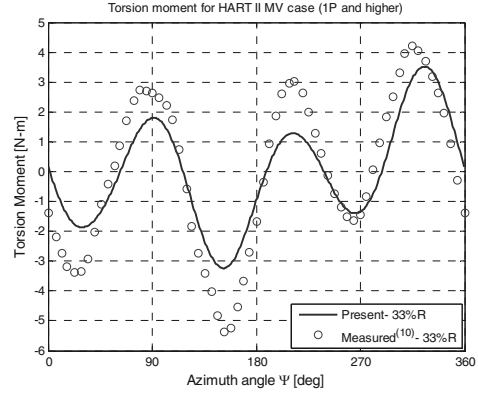
(a) 20% blade span



(b) Leadlag bending moments

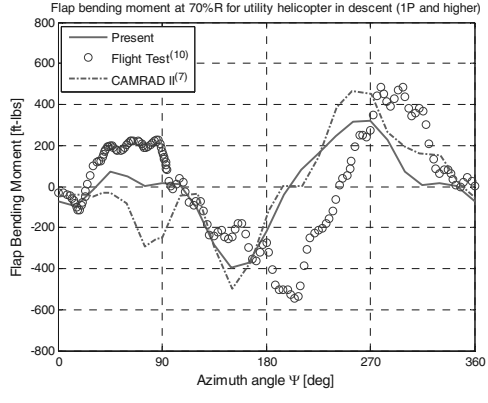


(b) 60% blade span



(c) Torsion moment

Figure 16. Correlation of blade structural loads for HART II MV case.



(c) 70% blade span

Figure 17. Correlation of flap bending moments for a utility helicopter in descent.

https://doi.org/10.1017/S0001924000006813 Published online by Cambridge University Press

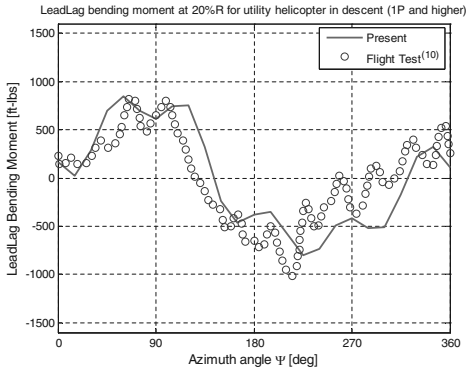


Figure 18. Correlation of leadlag bending moment for a utility helicopter in descent.

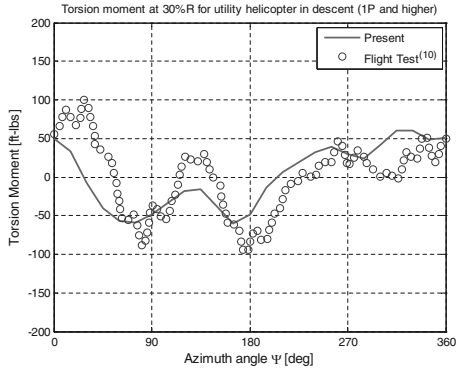


Figure 19. Correlation of torsion moments for a utility helicopter in descent.

extremely similar and the peak-to-peak magnitudes are significantly under-predicted. This under-prediction may be improved by introducing more sophisticated aerodynamics from CFD analysis. The measured lead-lag bending moments at the two radial locations are almost identical and have, approximately, a one-per-rev variation. The predicted lead-lag bending moments match reasonably with the measured data, but there are moderate discrepancies at around the azimuth angle of 180°. The torsion moment is predicted reasonably in terms of the waveform and the peak-to-peak magnitude.

Figures 15 and 16 show the blade structural loads for the MN and MV cases. The prediction characteristics are similar to the prediction results of the BL case. In both the MN and MV cases, the torsion moment prediction is more accurate than the correlations of the flap bending and lead-lag bending moments. Although the peak-to-peak value of the torsion moment is under-predicted, the three-per-rev variation is predicted well.

3.4.2 Utility helicopter

For a utility helicopter in descent, three flap bending moments at $r/R = 0{\cdot}2$, $0{\cdot}6$, and $0{\cdot}7$, one lead-lag bending moment at $r/R = 0{\cdot}2$, and one torsion moment at $r/R = 0{\cdot}3$ are compared with the measured values. Particularly, the predictions for the flap bending moments at $r/R = 0{\cdot}6$ and $0{\cdot}7$ are compared with the previous result of CAMRAD II with multiple trailer wakes[7] as well as the test data.

The correlations of the flap bending moments are given in Fig. 17. The waveforms at the three locations are predicted nicely but phase-lead phenomena is observed. Furthermore, the oscillations of the flap bending moments at $r/R = 0{\cdot}6$ and $0{\cdot}7$ are not captured well in both the predictions. However, the present waveform in the first quadrant is close to the measured data. The lead-lag bending moment as given in Figure 18 shows a fair prediction, though some of the oscillations are not captured. Figure 19 shows that the torsion moment is predicted well although the peak-to-peak magnitude is under-predicted. One of the reasons of the discrepancy between the present prediction and the measured data may be due to the inaccurate blade section properties.

https://doi.org/10.1017/S0001924000006813 Published online by Cambridge University Press

4.0 CONCLUSION

This paper studied the rotor aeromechanical behaviour in descending flight using the nonlinear flexible multibody dynamics analysis, DYMORE. The freewake model was included to improve the rotor wake capturing capability into the present comprehensive analysis. The full-scale utility helicopter rotor in descent as well as the HART II BL, MN and MV cases was considered in order to correlate the BVI airloads in the full range of the blade span with the measured data. Furthermore, the blade deformations of the HART II rotor and the blade structural loads of the HART II and utility helicopter rotors were correlated with the test results. From the present correlation study, the following conclusions were obtained:

1. The BVI airloads for both the HART II and utility helicopter rotors in descent were correlated fairly with the measured data although some of BVI events on the advancing side were missed for both the rotors.
2. The predicted lift distribution on the rotor disk of a utility helicopter in descent was similar to that of the HART II BL case. There were three lift peaks in the after of the rotor disk, and on the advancing and retreating sides.
3. The blade deformations at the tip for the HART II were correlated with the measured data. The flap deflections in the BL, MN and MV cases were predicted nicely. The prediction of the elastic torsion deformation in the BL case was not good since its peak-to-peak value was under-predicted significantly, although the wave form was captured reasonably. However, the elastic torsion deformations in both the MN and MV cases matched reasonably with the measured data.
4. The blade structural loads for the HART II and utility helicopter rotors were correlated with the test data. For the HART II rotor, the flap bending moment prediction was poor, the lead-lag bending moment correlation was fair, and the torsion moment prediction was reasonably satisfactory. For a utility helicopter rotor, the flap bending moment was predicted reasonably, although the slight phase shift was observed. The lead-lag bending moment matched well with the measured data. Particularly, the torsion moment correlation was satisfactory.
5. The present predictions for a utility helicopter rotor were also correlated well with the previous results by CAMRAD II with multiple trailer wakes. For the section lifts at the six blade stations, the present lift variations were quite similar to the CAMRAD II result. However the number of and the locations of the BVI events were predicted differently between the present DYMORE analysis and previous CAMRAD II prediction. For the flap bending moments at the 60% and 70% blade stations, the present predictions showed fair agreements with the previous CAMRAD II results.
6. In general, reasonable correlations were obtained with the present comprehensive multibody dynamics analysis. However, a coupled multibody/CFD analysis should be conducted for more accurate predictions, especially BVI airloads, in descending flights.

ACKNOWLEDGEMENTS

This work was supported by Leading Foreign Research Institute Recruitment Program though the National Research Foundation of Korea (NRF) funded by the Ministry of Education, Science and Technology (MEST) in 2011 (No. K20601000001). The first author would like to

https://doi.org/10.1017/S0001924000006813 Published online by Cambridge University Press

express his acknowledgement to Professor Bauchau at Georgia Institute of Technology, Dr Liu at Vestas Technology R&D Americas, Inc. and Dr Roget at National Institute of Aerospace (now Professor at University of Wyoming) for giving valuable help and advice to this work. Finally, the authors thank the HART II team for the test data.

REFERENCES

1. KUFELD, R.M., BALOUGH, D.L., CROSS, J.L., STUDEBAKER, K.F., JENNISON, C.D. and BOUSMAN, W. G. Flight testing the UH-60A Airloads Aircraft, Proceedings of the American Helicopter Society 50th Annual Forum, 1994.
2. YU, Y.-H., GMELIN, B., HELLER, H., PHILLIPPE, J.J., MERCKER, E. and PREISSER, J.S. HHC aeroacoustics rotor test at the DNW – The joint German/French/US HART project, Proceedings of 20th European Rotorcraft Forum, 1994.
3. YU, Y.-H., TUNG, C., VAN DER WALL, B.G., PAUSDER, H.-J., BURLEY, C., BROOKS, T., BEAUMIER, P., DELRIEUX, Y., MERCKER, E. and PENGEL, K. The HART-II test: rotor wakes aeroacoustics with Higher-Harmonic pitch Control (HHC) inputs – The joint German/French/Dutch/US project, Proceedings of the American Helicopter Society 58th Annual Forum, 2002.
4. NORMAN, T. R., SHINODA, P. M., KITAPLIOGLU, C., JACKLIN, S.A. and SHEIKMAN, A. Low-speed wind-tunnel investigation of a full-scale UH-60 rotor system, Proceedings of the American Helicopter Society 58th Annual Forum, 2002.
5. YEO, H.-S., ROMANDER, E.A. and NORMAN, T.R. Investigation of rotor performance and loads of a UH-60A individual blade control system, Proceedings of the American Helicopter Society 66th Annual Forum, 2010.
6. VAN DER WALL, B.G. 2nd HHC Aeroacoustic rotor test (HART II) – Part II: Representation results, Institute Report IB 111-2005/03, German Aerospace Center (DLR), Braunschweig, Germany, 2005.
7. LIM, J.-W. and VAN DER WALL, B.G. Investigation of the effect of a multiple trailer wake model for descending flights, Proceedings of the American Helicopter Society 61st Annual Forum, 2005.
8. SA, J.-H., KIM, J.-W., PARK, S.-H., PARK, J.-S., JUNG, S.N. and YU, Y.-H. KFLOW results of airloads on HART-II rotor blades with prescribed blade deformation, Proceedings of 2nd International Forum on Rotorcraft Multidisciplinary Technology, 2009.
9. LIM, J.-W., NYGAARD, T. A., STRAWN, R. and POTSDAM, M. BVI airloads prediction using CFD/CSD loose coupling, Proceedings of the American Helicopter Society 4th Vertical Lift Aircraft Design Conference, 2006.
10. LIM, J.-W. An assessment of rotor dynamics correlation for descending flight using CSD/CFD coupled analysis, Proceedings of the American Helicopter Society 64th Annual Forum, 2008.
11. JOHNSON, W. CAMRAD II, comprehensive analytical model of rotorcraft aerodynamics and dynamics, Johnson Aeronautics, 1992.
12. BAUCHAU, O.A. DYMORE manual (version 2.0): http://soliton.ae.gatech.edu/people/ obauchau/ Dwnld/dymore20/DymoreManual.pdf.
13. MANTEGAZZA, P. MBDYN: http://www.aero.polimi.it/~mbdyn.
14. SHIN, S.-J. Integral Twist Aactuation of Helicopter Rotor Blades for Vibration Reduction, PhD thesis, Massachusetts Institute of Technology, 2001.
15. ROGET, B. Simulation of active twist and active flap control on a model-scale helicopter rotor, Proceedings of 24th Applied Aerodynamics Conference, 2006.
16. PARK, J.-S., JUNG, S., PARK, S.-H. and YU, Y.-H. Correlation study of a rotor in descending flight using DYMORE with a freewake mode, *J Mechanical Science and Technology*, 2010, **24**, (8), pp 1583-1594.
17. SHEN, J., MASARATI, P., ROGET, B., PIATAK, D.J., NIXON, M.W. and SINGLETON, J.D. Stiff-inplane tiltrotor aeromechanics investigation using two multibody analyses, *Proceedings of Multibody Dynamics*, 2007.
18. HODGES, D.H. A mixed variational formulation based on exact intrinsic equations for dynamics of moving beams, *Int J Solids and Structures*, 1990, **26**, (11), pp 1253-1273.
19. PETERS, D.A. and HE, C.J. Finite state induced flow models Part II: Three-dimensional rotor disk, *J Aircr*, 1995, **32**, (2), pp 323-333.

https://doi.org/10.1017/S0001924000006813 Published online by Cambridge University Press

20· BHAGWAT, M.J. and LEISHMAN, J.G. Stability, consistency and convergence of time-marching free-vortex rotor wake algorithms, *J American Helicopter Society*, 2001, **46**, (1), pp 59-71.
21. VAN DER WALL, B.G. 2nd HHC Aeroacoustic rotor test (HART II) – Part I: Test document-, Institute Report IB 111-2003/31, German Aerospace Center (DLR), Braunschweig, Germany, 2003.
22. HOWLETT, J.J. UH-60A Black Hawk engineering simulation program: volume I – mathematical model, NASA Contractor Report 166309, 1981.
23. DAVIS, S.J. Predesign Study for a modern 4-bladed rotor for the RSRA, NASA Contractor Report 166155, 1981.
24. BAUCHAU, O.A. and LIU, H. On the modelling of hydraulic components in rotorcraft systems, *J American Helicopter Society*, 2006, **51**, (2), pp 175-184.
25. WELSH, W. Simulation and correlation of a helicopter air-oil strut dynamic response, Proceedings of American Helicopter Society 43rd Annual Forum, 1988.
26. DATTA, A. Fundamental Understanding, Prediction and Validation of Rotor Vibratory Loads in Steady Level Flight, PhD thesis, University of Maryland, Maryland, USA, 2004.
27. FLEMMING, R.J. An Experimental Evaluation of Advanced Rotorcraft Airfoils in the NASA Ames Eleven-Foot Transonic Wind Tunnel, NASA Contractor Report 166587, 1984.
28. MAYDA, E.A. A CFD-Based Methodology to Automate the Generation of C81 Airfoil Performance Tables, MS thesis, University of California, Davis, USA, 2003.
29. VAN RIPER, S.G. Investigation of Increased Forward Flight Velocities of Helicopters Using Higher Harmonic Stall Control and Reverse Velocity Rotor Concept, MS thesis, Naval Postgraduate School, 2003.
30· SITARAMAN, J. CFD Based Unsteady Aerodynamic Modelling for Rotor Aeroelastic Analysis, PhD thesis, University of Maryland, Maryland, USA, 2004.
31. NAVARRETE, J. Construction of Airfoil Performance Tables by the Fusion of Experimental and Numerical Data, MS thesis, Rice University, 2004.
32. ABRAS, J.N. Enhancement of Aeroelastic Rotor Airloads Prediction Methods, PhD thesis, Georgia Institute of Technology, Georgia, USA, 2009.
33. SQUIRE, H.B. The growth of a vortex in turbulent flow, *Aeronaut Quarterly*, 1965, **16**, pp 302-306.
34. RAMASAMY, M. and LEISHMAN, J.G. Reynolds number based blade tip vortex model, Proceedings of American Helicopter Society 61st Annual Forum, 2005.
35. HO, J.C., YEO, H.-S. and ORMISTON, R.A. Investigation of rotor blade structural dynamics and modelling based on measured airloads, *J Aircr*, 2008, **45**, (5), pp 1631-1642.

https://doi.org/10.1017/S0001924000006813 Published online by Cambridge University Press